Other Physics Opportunities with the ALERT Run Group

W. R. Armstrong[†], J. Arrington, I. Cloët, K. Hafidi[†‡], M. Hattawy[†], D. Potteveld, P. Reimer, Z. Yi

Argonne National Laboratory, Lemont, IL 60439, USA

J. Bettane, R. Dupré[†], M. Guidal, D. Marchand, C. Muñoz, S. Niccolai, E. Voutier

Institut de Physique Nucléaire, CNRS-IN2P3, Univ. Paris-Sud, Université Paris-Saclay, 91406 Orsay Cedex, France

M. J. Amaryan, G. Charles, G. Dodge

Old Dominion University, Norfolk, VA 23529, USA

N. Baltzell, S. Stepanyan

Thomas Jefferson National Accelerator Facility, Newport News, VA 23606, USA

B. Duran, S. Joosten, Z.-E. Meziani[†‡], M. Paolone[†], M. Rehfuss, N. Sparveris

Temple University, Philadelphia, PA 19122, USA

S. Liuti

University of Virginia, Charlottesville, VA 22903, USA

[†]Spokesperson
[‡]Contact person: kawtar@anl.gov
[‡]Contact person

Jefferson Lab PAC 45

Nuclear Exclusive and Semi-inclusive Measurements with a New CLAS12 Low Energy Recoil Tracker

ALERT Run Group[†]

EXECUTIVE SUMMARY

In this run group, we propose a comprehensive physics program to investigate the fundamental structure of the ^{4}He nucleus. An important focus of this program is on the coherent exclusive Deep Virtual Compton Scattering (DVCS) and Deep Virtual Meson Production (DVMP) with emphasis on ϕ meson production. These are particularly powerful tools enabling model-independent nuclear 3D tomography through the access of partons' position in the transverse plane. These exclusive measurements will give the chance to compare directly the quark and gluon radii of the helium nucleus. Another important measurement proposed in this program is the study of the partonic structure of bound nucleons. To this end, we propose next generation nuclear measurements in which low energy recoil nuclei are detected. The tagging of recoil nuclei in deep inelastic reactions is a powerful technique, which will provide unique information about the nature of medium modifications through the measurement of the EMC ratio and its dependence on the nucleon off-shellness. Finally, we propose to measure incoherent spectator-tagged DVCS on light nuclei (d, ^{4}He) where the observables are sensitive to the Generalized Parton Distributions (GPDs) of a quasi-free neutron for the case of the deuteron, and bound proton and neutron for the case of ^{4}He. The objective is to study and separate nuclear effects and their manifestation in GPDs. The fully exclusive kinematics provide a novel approach for studying final state interactions in the measurements of the beam spin asymmetries and the off-forward EMC ratio.

At the heart of this program is the Low Energy Recoil Tracker (ALERT) combined with the CLAS12 detector. The ALERT detector is composed of a stereo drift chamber for track reconstruction and an array of scintillators for particle identification. Coupling these two types of fast detectors will allow ALERT to be included in the trigger for efficient

[†]Contact Person: Kawtar Hafidi (kawtar@anl.gov)

background rejection, while keeping the material budget as low as possible for low energy particle detection. ALERT will be installed inside the solenoid magnet instead of the CLAS12 Silicon Vertex Tracker and Micromegas tracker. We will use an 11 GeV longitudinally polarized electron beam (80% polarization) of up to 1000 nA on a gas target straw filled with deuterium or ^{4}He at 3 atm to obtain a luminosity up to 6×10^{34} nucleon cm^{-2}s^{-1}. In addition we will need to run hydrogen and ^{4}He targets at different beam energies for detector calibration. The following table summarizes our beam time request:

Configurations	**Proposals**	**Targets**	**Beam time request**	**Beam current**	**Luminosity***
			days	nA	n/cm^2/s
Commissioning	All†	^{1}H, ^{4}He	5	Various	Various
A	Nuclear GPDs	^{4}He	10	1000	6×10^{34}
B	Tagged EMC & DVCS	^{2}H	20	500	3×10^{34}
C	All†	^{4}He	20	500	3×10^{34}
TOTAL			**55**		

*This luminosity value is based on the effective part of the target. When accounting for the target's windows, which are outside of the ALERT detector, it is increased by 60%.

†"All" includes the four proposals of the run group: Nuclear GPDs, Tagged EMC, Tagged DVCS and Extra Topics. Note that the beam time request is only driven by the three first proposals.

Abstract

This proposal summarizes some additional physics measurements that can be done as part of the ALERT run group without need for new beam time. There is indeed a tremendous potential for this data, which can advance our understanding of QCD on several fronts including the partonic structure of the nucleon and the nucleus, the modification of the nucleon structure in the nuclear medium, the nuclear final state interactions and meson spectroscopy. The key to achieving success in all these areas is the detection of the recoil fragments, which is possible with the proposed low energy recoil tracker (ALERT).

As a complementary measurement to "the partonic structure of light nuclei" proposal, which focuses on deep virtual Compton scattering (DVCS) off ^{4}He nucleus, we propose to extend the measurement to the deuteron. This will allow us, for the first time, to measure in an exclusive way DVCS off deuterium to shed light on its partonic structure. For deep virtual meson production (DVMP) measurements, we would like to extend the ϕ measurements to the π^0 meson, which will allow access to the ^{4}He single chiral-odd GPD H_T. Finally, we propose to measure DVCS in three-body break up reactions, which will be a natural extension of the "Tagged DVCS off light nuclei" proposal.

This fourth proposal shows our every intention to fully exploit the data collected during the ALERT run group because of its uniqueness and the potential it has to enable breakthroughs in our understanding of nuclear QCD.

Contents

Introduction

The combination of the high luminosity available at Jefferson Lab, the large acceptance of CLAS12 detector and the low energy recoil tracker (ALERT) offers an amazing opportunity to advance our understanding of long standing mysteries in nuclear QCD. Moreover, the ability to detect low energy recoil fragments is crucial to control final state interactions (FSI) which spoil most of the semi-inclusive measurements. The recoil detector ALERT is also very interesting for coherent reactions which are difficult to identify on nuclear targets based only on kinematics. The direct detection of the recoil nuclei is then a guaranty of the coherence of the process.

This new development in detection capabilities, will allow the study of medium modification with a handle on Fermi motion uncertainties and FSI effects. It is therefore clear that the focus of the three main proposals of the ALERT run group is only a fraction of the physics that can be achieved by successfully analyzing the ALERT run group data. This data will be a gold mine, which will allow us to investigate in a unique way several important physics questions and conquer new territories in the nuclear QCD land. These are examples of physics that can be studied with the ALERT data. Some of the topics were included in the JLab letter of intent LOI-10-009 [1] submitted to PAC35:

- Coherent DVCS and DVMP off deuteron. For DVMP, we can study for example π^0, ϕ, ω and ρ mesons.
- Deep virtual π^0 production off ^{4}He, which is interesting by itself but also the background of DVCS measurements.
- Semi-inclusive reaction p(e,e'p)X to study the π^0 cloud of the proton and $D(e, e'pp_S)X$ to study the π^- cloud of the neutron, at very low proton momenta.
- Meson spectroscopy in coherent production off ^{4}He as an extension of the exploratory measurements during eg6 experiment E-07-009. Coherent production is used to eliminate physics background arising from associated baryon resonance production. In order to ensure coherent production of a mesonic state, the recoil nuclei must be detected.
- Tagged nuclear form factors measurements.
- The role of Δs in short-range correlations.

- The role of the final state interaction in hadronization and medium modified fragmentation functions.
- The medium modification of the transverse momentum dependent parton distributions.

For practical reasons, we are focusing here on three topics only. These are closely connected to the three proposals, which form the ALERT run group. These topics are exclusive π^0 production off ^{4}He, coherent exclusive DVCS off deuteron and DVCS in three-body break up reactions.

Chapter 1

Summary of Physics Topics

1.1 Helium GPDs beyond the DVCS at leading order and leading twist

A wealth of information on the QCD structure of hadrons lies in the correlations between the momentum and spatial degrees of freedom of the constituent partons. Such correlations are accessible via GPDs which, more specifically, describe the longitudinal momentum distribution of a parton located at a given position in the transverse plane. The processes which are most directly related to GPDs are DVCS and DVMP corresponding to the exclusive electroproduction of a real photon or a meson, respectively.

GPDs provide essential information for determining the missing component to the nucleon *longitudinal* spin sum rule in the kinematic setting where the proton moves in the z direction, its spin being polarized along the same direction. A complete description of nucleon structure requires, however, understanding also the *transverse* spin ([2] and references therein). An experimental determination of the chiral-odd quark helicity-flip GPDs, $H_T(x,\xi,t), E_T(x,\xi,t), \tilde{H}_T(x,\xi,t)$, and $\tilde{E}_T(x,\xi,t)$ [3] is crucial for this effort.

In Ref.[4], it was suggested that deeply virtual exclusive pseudoscalar electroproduction can provide a direct channel to measure chiral-odd GPDs so long as the helicity flip contribution to the quark-pion vertex is dominant. This idea was subsequently endorsed and further developed in Refs.[5, 6, 7, 8, 9]. Recently, experimental measurements from Jefferson Lab have been interpreted in terms of chiral odd GPDs [10, 11, 12]. In particular, by measuring separately π^o and η production [11], it is possible to perform a flavor separated analysis of the chiral odd GPDs. As pointed out in [7, 13], however, in principle all four chiral odd GPDs enter the description of the various terms in the nucleon cross section. It is therefore a tantalizing job to disentangle their various contributions.

The number of GPDs needed to parametrize the partonic structure of a nucleus depends

on the different configurations between the spin of the nucleus and the helicity direction of the struck quark. For example, for a target of spin s, the number of chiral-even GPDs is equal to $(2s+1)^2$ for each quark flavor. DVCS off spinless nuclear targets, such as ^{4}He, ^{12}C and ^{16}O, is simpler to study since only a chiral-even GPD, H_A, and a chiral-odd GPD, H_A^T, are present at leading twist and two chiral even GPDs, $H_A^{(3)}$, and $\tilde{H}_A^{(3)}$, arise at twist three. This limited number of GPDs make it much simpler to interpret data from observables linked to these extra GPDs using a spin less target.

The ^{4}He nucleus, characterized by its high density can be considered as the smallest of complex nuclei. Moreover, inclusive scattering off ^{4}He shows a large EMC effect. Therefore, this nucleus represents an ideal target for understanding a variety of nuclear effects through GPDs measurements. The twist three GPDs, $H_A^{(3)}$ and $\tilde{H}_A^{(3)}$, allow us to access the so far unexplored spin correlation of a longitudinally polarized quark in an unpolarized target. This, in turn, would give us unique information on the quark spin-orbit interaction, $\vec{S}\cdot\vec{L}$, in a nuclear environment [14]. We recall, again, that for a spin zero target the twist three GPDs are much easier to disentangle than in a nucleon, since the description of the latter requires a larger number of functions. The chiral-odd GPD, H_A^T, measured through deeply virtual π^0 production (background to DVCS signal) can be expressed in the low ξ approximation, as a convolution over the transversity GPD, H_T. The latter becomes the transversity PDF, h_1, in the forward limit. Measurements of nuclear medium modifications of this quantity would be crucial for further exploring the hypothesis originally put forward in Ref. [15] of whether the EMC effect is enhanced in spin dependent observables.

We propose to measure coherent deep exclusive π^0 BSA off ^{4}He to extract both the real and imaginary part of chiral-odd nuclear Compton form factors H_A^T and investigate the sensitivity to twist-3 contributions. The corresponding formalism is described in details in Appendix A.

1.2 Coherent exclusive DVCS off deuteron

Deep inelastic scattering processes in the deuteron have been used mainly as the source of information on unpolarized and polarized distributions of a neutron in the forward limit. With the advent of DVCS it became possible to study GPDs of a deuteron as a whole leaving it intact in the final state. Due to the fact that it is a spin-1 object, there are entirely new functions appearing, which could give us a deeper understanding of this nucleus in terms of its fundamental degrees of freedom. The nine GPDs for a spin-1 object have been given in Ref. [16] and their properties have been discussed in detail in Ref. [17]. Sum rules relate these GPDs to the usual deuteron form factors $G_i (i = 1, 3)$, which are linear combinations of charge monopole G_C, magnetic dipole G_M , and charge quadrupole, G_Q. The unique feature of these relations is the fact that the $G_3(t)$ form factor is totally dominated by the charge quadrupole $G_Q(t)$ [18] and allows us to access the H_3 GPD via beam-spin asymmetry

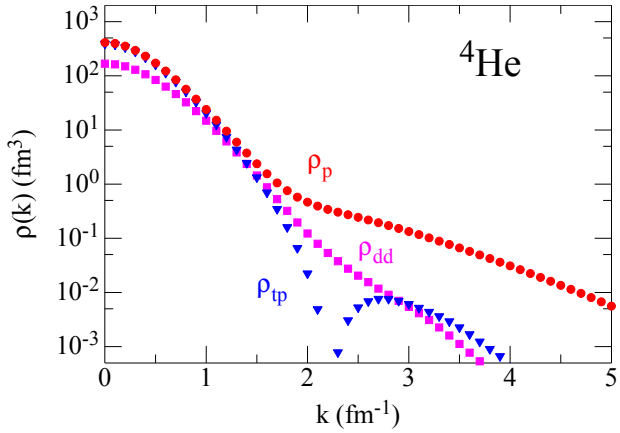

Figure 1.1: The proton momentum distribution in ^{4}He is shown by the red circles; the *tp* cluster distribution is shown by the blue triangles and the *dd* cluster distribution is shown by the magenta squares. [19]

measurements. This will be the first measurement of the partonic structure function of the deuteron related in the forward limit to charge quadrupole, and not only to the charge and the magnetic form factors, which can not be decomposed into simple additive sum of the proton and the neutron. Using the results of these measurements, we can access the partonic structure of the deuteron treated as a single hadron, which is irreducible to the partonic structure of its nucleon constituents.

We propose here to measure the beam-spin asymmetries of the coherent DVCS scattering process on a deuteron target using CLAS12 to detect the scattered electron and the high energy photon and the ALERT detector to detect low energy recoil deuterons. This data will help determine our sensitivity to the charge quadrupole in coherent DVCS off deuteron and possibly motivate future proposals.

1.3 DVCS in three-body break up reactions

The three-body break up (3BBU) reactions are of particular interest in nuclear physics because they provide information about the substructure and nucleon correlations within a nucleus. For example quasi-elastic knock-out of a neutron from ^{4}He leaves the remaining three nucleon system behind but the degree to which it remains a ^{3}He depends on the initial nuclear configuration and final state interactions. As shown in Figure 1.1, when going to larger momenta, finding a recoil triton becomes unlikely and 3BBU configurations start to dominate. Our detector setup allows to detect multiple recoil fragments and CLAS12 will be equipped with a central neutron detector (CND) making possible to detect final states where ^{4}He $\rightarrow$ d+p+n.

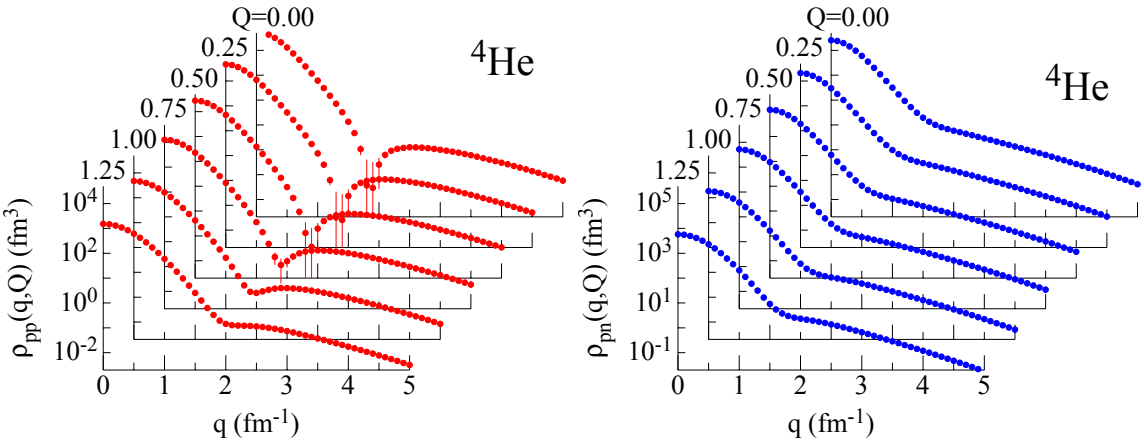

Figure 1.2: The proton-proton (left) and the proton-neutron (right) momentum distributions in ^{4}He averaged over the directions of $\boldsymbol{q} = (\boldsymbol{k}_1 - \boldsymbol{k}_2)/2$ and $\boldsymbol{Q} = \boldsymbol{k}_1 + \boldsymbol{k}_2$ as a function of q for several fixed values of Q. Reproduced from Ref. [19].

This study can be made similarly for DVCS, asymmetries appears to be rather simple observables to extract within the experimental conditions of this run group. This partonic level measurement can be used to access not only the parton distributions of the bound nucleon, but also the parton distributions for specific configurations of the nucleus. This can be understood by considering the relative motion of correlated pairs inside of the ^{4}He nucleus as shown in Figure 1.2.

We propose here to measure the beam-spin asymmetries of the DVCS scattering in three-body break up reactions off ^{4}He target using CLAS12 to detect the scattered electron, neutrons and the high energy photon and the ALERT detector to detect low energy recoil fragments.

Chapter 2

Experimental Setup

All the different measurements of the ALERT run group require, in addition to a good scattered electron measurement, the detection of low energy nuclear recoil fragments with a large kinematic coverage. Such measurements have been performed in CLAS (BONuS and eg6 runs), where the adequacy of a small additional detector placed in the center of CLAS right around the target has shown to be the best solution. We propose here a similar setup using the CLAS12 spectrometer augmented by a low energy recoil detector.

We summarize in Table 2.1 the requirements for the different experiments proposed in the run group. By comparison with previous similar experiments, the proposed tagged measurements necessitate a good particle identification. Also, CLAS12 will be able to handle higher luminosity than CLAS so it will be key to exploit this feature in the future setting in order to keep our beam time request reasonable.

Measurement	Particles detected	p range	θ range
Nuclear GPDs	^{4}He	$230 < p < 400 MeV/c$	$\pi/4 < \theta < \pi/2$ rad
Tagged EMC	p, ^{3}H, ^{3}He	As low as possible	As close to π as possible
Tagged DVCS	p, ^{3}H, ^{3}He	As low as possible	As close to π as possible

Table 2.1: Requirements for the detection of low momentum spectator fragments of the proposed measurements.

This chapter will begin with a brief description of CLAS12. After presenting the existing options for recoil detection and recognize that they will not fulfill the needs laid out above, we will describe the design of the proposed new recoil detector ALERT. We will then present the reconstruction scheme of ALERT and show the first prototypes built by our technical

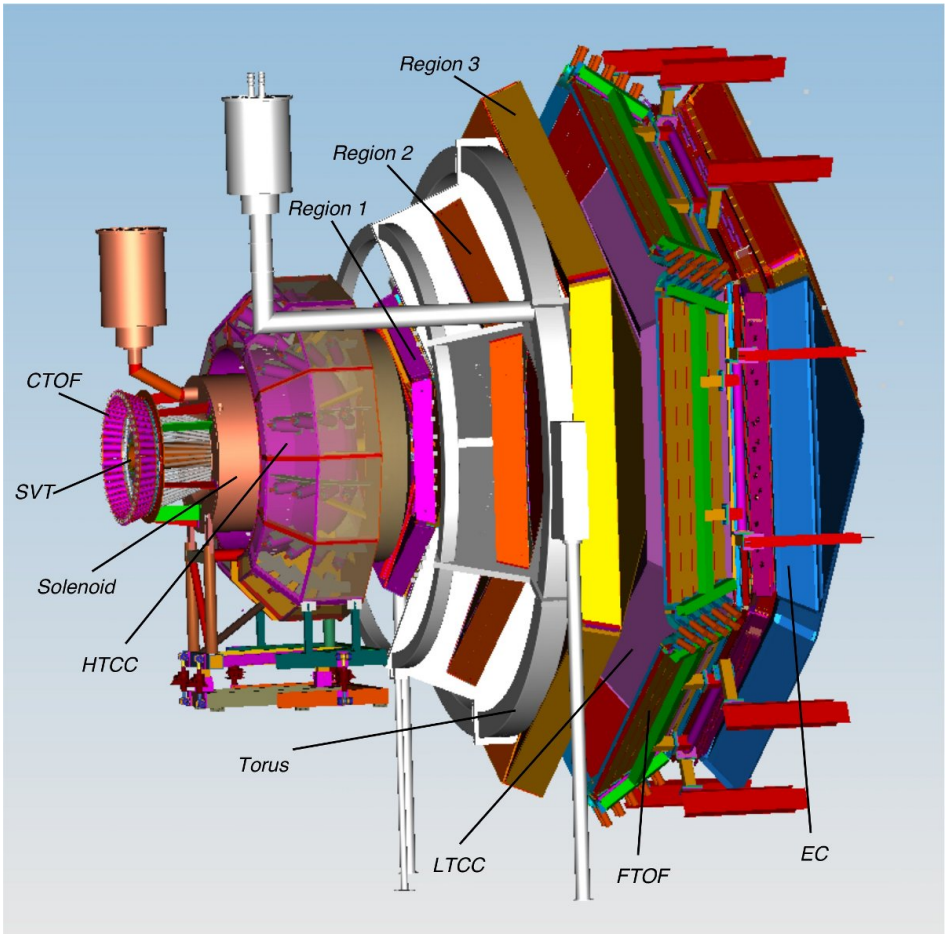

Figure 2.1: The schematic layout of the CLAS12 baseline design.

teams. Finally, we specify the technical contributions of the different partners.

2.1 The CLAS12 Spectrometer

The CLAS12 detector is designed to operate with 11 GeV beam at an electron-nucleon luminosity of $\mathcal{L} = 1 \times 10^{35}$ cm^{-2}s^{-1}. The baseline configuration of the CLAS12 detector consists of the forward detector and the central detector packages [20] (see Figure 2.1). We use the forward detector for electron detection in all ALERT run group proposals, while DVCS centered proposals also use it for photon detection. The central detector's silicon tracker and micromegas will be removed to leave room for the recoil detector.

The scattered electrons and photons will be detected in the forward detector which consists of the High Threshold Cherenkov Counters (HTCC), Drift Chambers (DC), the Low Threshold Cherenkov Counters (LTCC), the Time-of-Flight scintillators (TOF), the Forward Calorimeter and the Preshower Calorimeter. The charged particle identification in the forward detector is achieved by utilizing the combination of the HTCC, LTCC and TOF arrays with the tracking information from the Drift Chambers. The HTCC together with the Forward Calorimeter and the Preshower Calorimeter will provide a pion rejection factor of more than 2000 up to a momentum of 4.9 GeV/c, and a rejection factor of 100 above 4.9 GeV/c. The photons are detected using the calorimeters.

2.2 Available options for a Low Energy Recoil Detector

We explored available solutions for the low-energy recoil tracker with adequate momentum and spatial resolution, and good particle identification for recoiling light nuclei (p, ^{3}H and ^{3}He). After investigating the feasibility of the proposed measurements using the CLAS12 Central Detector and the BONuS Detector [21, 22], we concluded that we needed to build a dedicated detector. We summarize in the following the facts that led us to this conclusion.

2.2.1 CLAS12 Central Detector

The CLAS12 Central Detector [20] is designed to detect various charged particles over a wide momentum and angular range. The main detector package includes:

- Solenoid Magnet: provides a central longitudinal magnetic field up to 5 Tesla, which serves to curl emitted low energy Møller electrons and determine particle momenta through tracking in the central detector.
- Central Tracker: consists of 3 double layers of silicon strips and 6 layers of Micromegas. The thickness of a single silicon layer is 320 µm.
- Central Time-of-Flight: an array of scintillator paddles with a cylindrical geometry of radius 26 cm and length 50 cm; the thickness of the detector is 2 cm with designed timing resolution of $\sigma_t = 50$ ps, used to separate pions and protons up to 1.2 GeV/c.

The current design, however, is not optimal for low energy particles ($p < 300$ MeV/c) due to the energy loss in the first 2 silicon strip layers. The momentum detection threshold is ~ 200 MeV/c for protons, ~ 350 MeV/c for deuterons and even higher for ^{3}H and ^{3}He. These values are significantly too large for any of the ALERT run group proposals.

Detector Property	RTPC	ALERT
Detection region radius	4 cm	5 cm
Longitudinal length	$\sim$ 40 cm	$\sim$ 30 cm
Gas mixture	80% helium/20% DME	90% helium/10% isobutane
Azimuthal coverage	360°	340°
Momentum range	70-250 MeV/c protons	70-250 MeV/c protons
Transverse mom. resolution	10% for 100 MeV/c protons	10% for 100 MeV/c protons
z resolution	3 mm	3 mm
Solenoidal field	$\sim$ 5 T	$\sim$ 5 T
ID of all light nuclei	No	Yes
Luminosity	3×10^{33} nucleon/cm^2/s	6×10^{34} nucleon/cm^2/s
Trigger	can not be included	can be included

Table 2.2: Comparison between the RTPC (left column) and the new tracker (right column).

2.2.2 BONuS12 Radial Time Projection Chamber

The original BONuS detector was built for Hall B experiment E03-012 to study neutron structure at high x_B by scattering electrons off an almost on-shell neutron inside deuteron. The purpose of the detector was to tag the low energy recoil protons ($p > 60$ MeV/c). The key component for detecting the slow protons was the Radial Time Projection Chamber (RTPC) based on Gas Electron Multipliers (GEM). A later run period (eg6) used a newly built RTPC with a new design to detect recoiling α particles in coherent DVCS scattering. The major improvements of the eg6 RTPC were full cylindrical coverage and a higher data taking rate.

The approved 12 GeV BONuS (BONuS12) experiment is planning to use a similar device with some upgrades. The target gas cell length will be doubled, and the new RTPC will be longer as well, therefore doubling the luminosity and increasing the acceptance. Taking advantage of the larger bore ($\sim$ 700 mm) of the 5 Tesla solenoid magnet, the maximum radial drift length will be increased from the present 3 cm to 4 cm, improving the momentum resolution by 50% [22] and extending the momentum coverage. The main features of the proposed BONuS12 detector are summarized in Table 2.2.

In principle, particle identification can be obtained from the RTPC through the energy loss dE/dx in the detector as a function of the particle momentum (see Figure 2.2). However, with such a small difference between ^{3}H and ^{3}He, it is nearly impossible to discriminate between them on an event by event basis because of the intrinsic width of the dE/dx distributions.

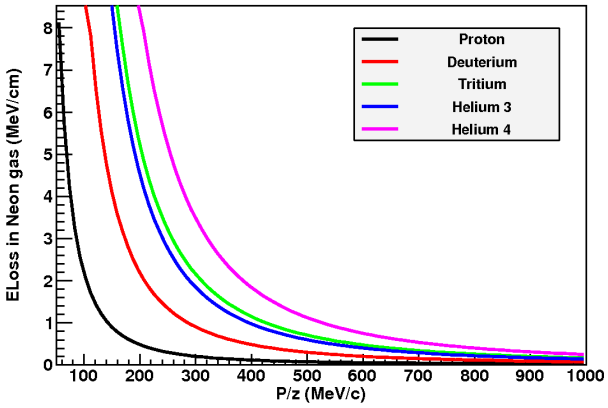

Figure 2.2: Calculation of energy loss in Neon gas as a function of the particle momentum divided by its charge for different nuclei.

This feature is not problematic when using deuterium target, but makes the RTPC no longer a viable option for our tagged EMC and tagged DVCS measurements which require a ^{4}He target and the differentiation of ^{4}He, ^{3}He, ^{3}H, deuterons and protons.

Another issue with the RTPC is its slow response time due to a long drift time (~ 5 μs). If a fast recoil detector could be included in the trigger it would have a significant impact on the background rejection. Indeed, in about 90% of DIS events on deuteron or helium, the spectator fragments have too low energy or too small angle to get out of the target and be detected. By including the recoil detector in the trigger, we would not be recording these events anymore. Since the data acquisition speed was the main limiting factor for both BONuS and eg6 runs in CLAS, this would be a much needed reduction of the pressure on the DAQ.

2.2.3 Summary

In summary, we found that the threshold of the CLAS12 inner tracker is significantly too high to be used for our measurements. On the other hand, the recoil detector planned for BONuS12, a RTPC, is not suitable due to its inability to distinguish all kind of particles we need to measure. Moreover, as the RTPC cannot be efficiently included in the trigger, a lot of background events are sent to the readout electronics, which will cause its saturation and limit the maximum luminosity the detector can handle. Therefore, we propose a new detector design.

2.3 Design of the ALERT Detector

We propose to build a low energy recoil detector consisting of two sub-systems: a drift chamber and a scintillator hodoscope. The drift chamber will be composed of 8 layers of sense wires to provide tracking information while the scintillators will provide particle identification through time-of-flight and energy measurements. To reduce the material budget, thus reducing the threshold to detect recoil particles at as low energy as possible, the scintillator hodoscope will be placed inside the gas chamber, just outside of the last layer of drift wires.

The drift chamber volume will be filled with a light gas mixture (90% He and 10% C_4H_{10}) at atmospheric pressure. The amplification potential will be kept low enough in order to not be sensitive to relativistic particles such as electrons and pions. Furthermore, a light gas mixture will increase the drift speed of the electrons from ionization. This will allow the chamber to withstand higher rates and experience lower hit occupancy. The fast signals from the chamber and the scintillators will be used in coincidence with electron trigger from CLAS12 to reduce the overall DAQ trigger rate and allow for operation at high luminosity.

The detector is designed to fit inside the central TOF of CLAS12; the silicon vertex tracker and the micromegas vertex tracker (MVT) will be removed. The available space has thus an outer radius of slightly more than 20 cm. A schematic layout of the preliminary design is shown in Figure 2.3 and its characteristics compared to the RTPC design in Table 2.2. The different detection elements are covering about 340° of the polar angle to leave room for mechanics, and are 30 cm long with an effort made to reduce the particle energy loss through the materials. From the inside out, it is composed of:

- a 30 cm long cylindrical target with an outer radius of 6 mm and target walls 25 µm Kapton filled with 3 atm of helium;
- a clear space filled with helium to reduce secondary scattering from the high rate Møller electrons with an outer radius of 30 mm;
- the drift chamber, its inner radius is 32 mm and its outer radius is 85 mm;
- two rings of plastic scintillators placed inside the gaseous chamber, with total thickness of roughly 20 mm.

2.3.1 The Drift Chamber

While drift chambers are very useful to cover large areas at a moderate price, huge progress has been made in terms of their ability to withstand higher rates using better electronics,

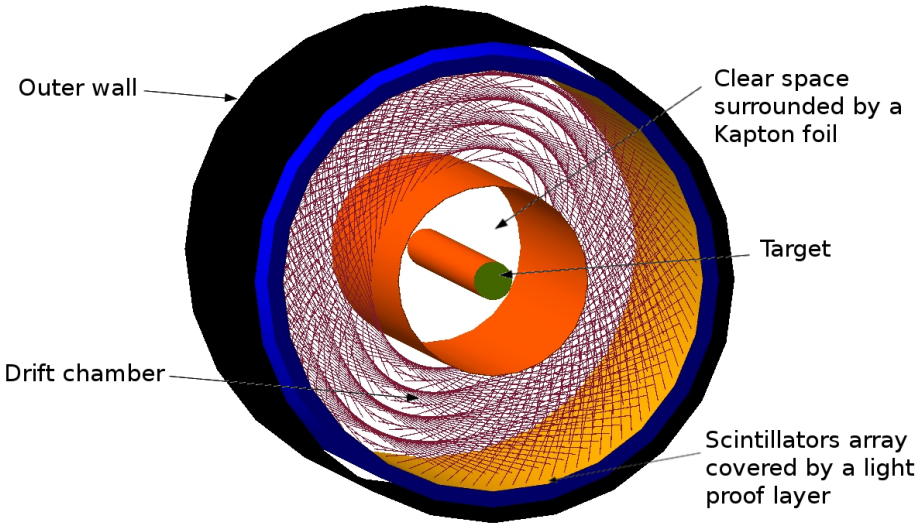

Figure 2.3: The schematic layout of the ALERT detector design, viewed from the beam direction.

shorter distance between wires and optimization of the electric field over pressure ratio. Our design is based on other chambers developed recently. For example for the dimuon arm of ALICE at CERN, drift chambers with cathode planes were built in Orsay [23]. The gap between sense wires is 2.1 mm and the distance between two cathode planes is also 2.1 mm, the wires are stretched over about 1 m. Belle II is building a cylindrical drift chamber very similar to what is needed for this experiment and for which the space between wires is around 2.5 mm [24]. Finally, a drift chamber with wire gaps of 1 mm is being built for the small wheel of ATLAS at CERN [25]. The cylindrical drift chamber proposed for our experiment is 300 mm long, and we therefore considered that a 2 mm gap between wires is technically a rather conservative goal. Optimization is envisioned based on experience with prototypes.

The radial form of the detector does not allow for 90 degrees x-y wires in the chamber. Thus, the wires of each layer are at alternating angle of $\pm$ 10°, called the stereo-angle, from the axis of the drift chamber. We use stereo-angles between wires to determine the coordinate along the beam axis (z). This setting makes it possible to use a thin forward end-plate to reduce multiple scattering of the outgoing high-energy electrons. A rough estimate of the tension due to the $\sim$2600 wires is under 600 kg, which appears to be reasonable for a composite end-plate.

The drift chamber cells are composed of one sense wire made of gold plated tungsten surrounded by field wires, however the presence of the 5 T magnetic field complicates the field lines. Several cell configurations have been studied with MAGBOLTZ [26], we decided

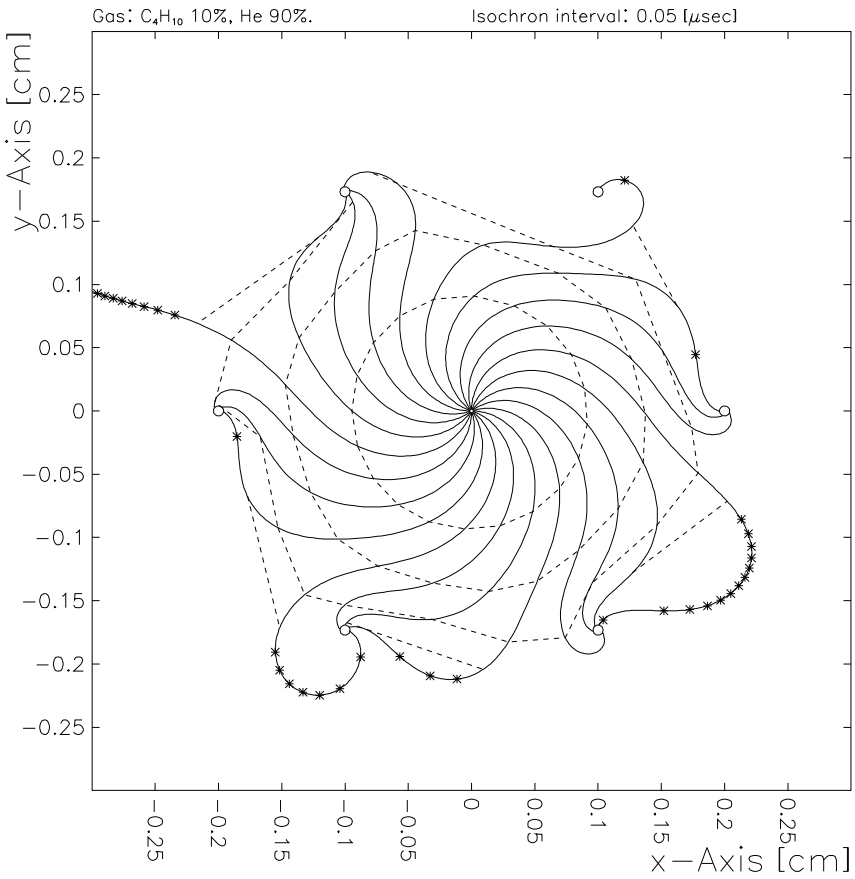

Figure 2.4: Drift lines simulated using MAGBOLTZ [26] for one sense wire (at the center) surrounded by 6 field wires. The two electric field lines leaving the cell disappear when adjusting the voltages on the wires. Dashed lines are isochrones spaced by 50 ns. This shows that the maximum drift time is about 250 ns.

to choose a conservative configuration as shown in Figure 2.4. The sense wire is surrounded by 6 field wires placed equidistantly from it in a hexagonal pattern. The distance between the sense and field wires is constant and equal to 2 mm. Two adjacent cells share the field wires placed between them. The current design will have 8 layers of cells of similar radius. The simulation code MAGBOLTZ is calculating the drift speed and drift paths of the electrons (Figure 2.4). With a moderate electric field, the drift speed is around 10 microns/ns, the average drift time expected is thus 250 ns (over 2 mm). Assuming a conservative 10 ns time resolution, the spatial resolution is expected to be around 200 microns due to field distortions and spread of the signal.

The maximum occupancy, shown in Figure 2.5, is expected to be around 5% for the inner most wires at 10^{35} $cm^{-2}s^{-1}$ (including the target windows). This is the maximum

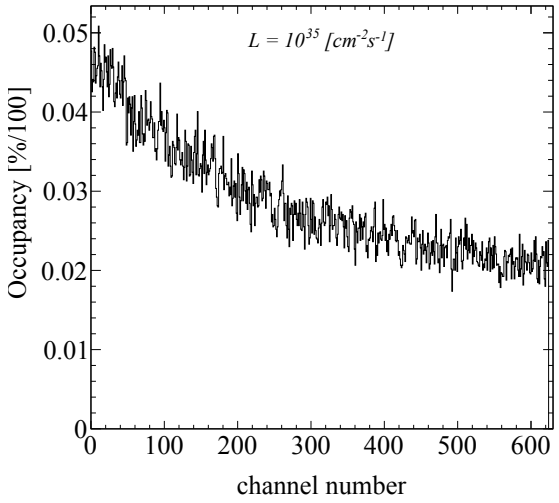

Figure 2.5: A full Geant4 simulation of the ALERT drift chamber hit occupancy at a luminosity of 10^{35} cm^{-2}s^{-1}. The channel numbering starts with the inner most wires and works outwards.

available luminosity for the baseline CLAS12 and is obtained based on the physics channels depicted in Figure 2.6, assuming an integration time of 200 ns and considering a readout wire separation of 4 mm. This amount of accidental hits does not appear to be reasonable for a good tracking quality, we therefore decided to run only at half this luminosity for our main production runs. This will keep occupancy below 3%, which is a reasonable amount for a drift chamber to maintain high tracking efficiency. When running the coherent processes with the ^{4}He target, it is not necessary to detect the protons[1], so the rate of accidental hits can then be highly reduced by increasing the detection threshold, thus making the chamber blind to the protons[2]. In this configuration, considering that our main contribution to occupancy are quasi-elastic protons, we are confident that the ALERT can work properly at 10^{35} cm^{-2}s^{-1}.

We are currently planning to use the electronics used by the MVT of CLAS12, known as the DREAM chip [27]. Its dynamic range and time resolution correspond to the needs of our drift chamber. To ensure that it is the case, tests with a prototype will be performed at the IPN Orsay (see section 2.5).

[1] This running condition is specific to the proposal "Partonic Structure of Light Nuclei" in the ALERT run group.

[2] The CLAS *eg6* run period was using the RTPC in the same fashion.

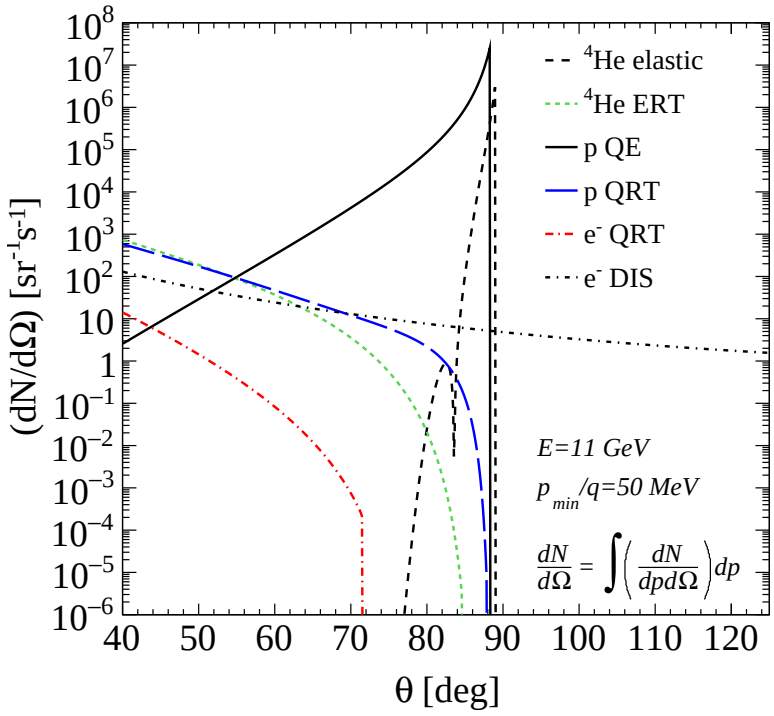

Figure 2.6: The rates for different processes as function of angle. The quasi-elastic radiative tails (QRT), ^{4}He elastic radiative tail (ERT), and DIS contributions have been integrated over momenta starting at $p/q = 50$ MeV/c, where q is the electric charge of the particle detected.

2.3.2 The Scintillator Array

The scintillator array will serve two main purposes. First, it will provide a useful complementary trigger signal because of its very fast response time, which will reduce the random background triggers. Second, it will provide particle identification, primarily through a time-of-flight measurement, but also by a measurement of the particle total energy deposited and path length in the scintillator which is important for doubly charged ions.

The length of the scintillators cannot exceed roughly 40 cm to keep the time resolution below 150 ps. It must also be segmented to match with tracks reconstructed in the drift chamber. Since ^{3}He and ^{4}He will travel at most a few mm in the scintillator for the highest anticipated momenta ($\sim$ 400 MeV/c), a multi-layer scintillator design provides an extra handle on particle identification by checking if the range exceeded the thickness of the first scintillator layer.

The initial scintillator design consists of a thin (2 mm) inner layer of 60 bars, 30 cm in length, and 600 segmented outer scintillators (10 segments 3 cm long for each inner bar) wrapped around the drift chamber. Each of these thin inner bars has SiPM[3] detectors attached to both ends. A thicker outer layer (18 mm) will be further segmented along the beam axis to provide position information and maintain good time resolution.

For the outer layer, a dual ended bar design and a tile design with embedded wavelength shifting fiber readouts similar to the forward tagger's hodoscope for CLAS12 [28] were considered. After simulating these designs, it was found that the time resolution was insufficient except only for the smallest of tile designs ($15\times15\times7$ mm^3). Instead of using fibers, a SiPM will be mounted directly on the outer layer of a keystone shaped scintillator that is 30 mm in length and 18 mm thick. This design can be seen in Figure 2.7 which shows a full Geant4 simulation of the drift chamber and scintillators. By directly mounting the SiPMs to the scintillator we collect the maximum signal in the shortest amount of time. With the large number of photons we expect, the time resolution of SiPMs will be a few tens of ps, which is well within our target.

The advantage of a dual ended readout is that the time sum is proportional to the TOF plus a constant. The improved separation of different particles can be seen in Figure 2.8. Reconstructing the position of a hit along the length of a bar in the first layer is important for the doubly charged ions because they will not penetrate deep enough to reach the second layer of segmented scintillator.

[3]SiPM: silicon photomultiplier.

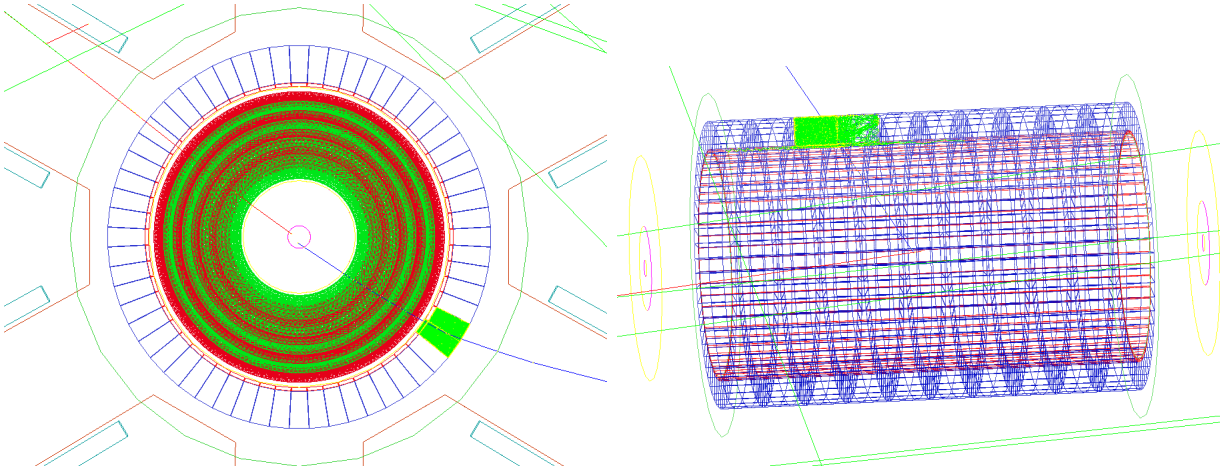

Figure 2.7: Geant4 simulation of a proton passing through the recoil drift chamber and scintillator hodoscope. The view looking downstream (left) shows the drift chamber's eight alternating layers of wires (green and red) surrounded by the two layers of scintillator (red and blue). Simulating a proton through the detector, photons (green) are produced in a few scintillators. On the right figure, the dark blue rings are graphical feature showing the contact between the adjacent outer scintillators.

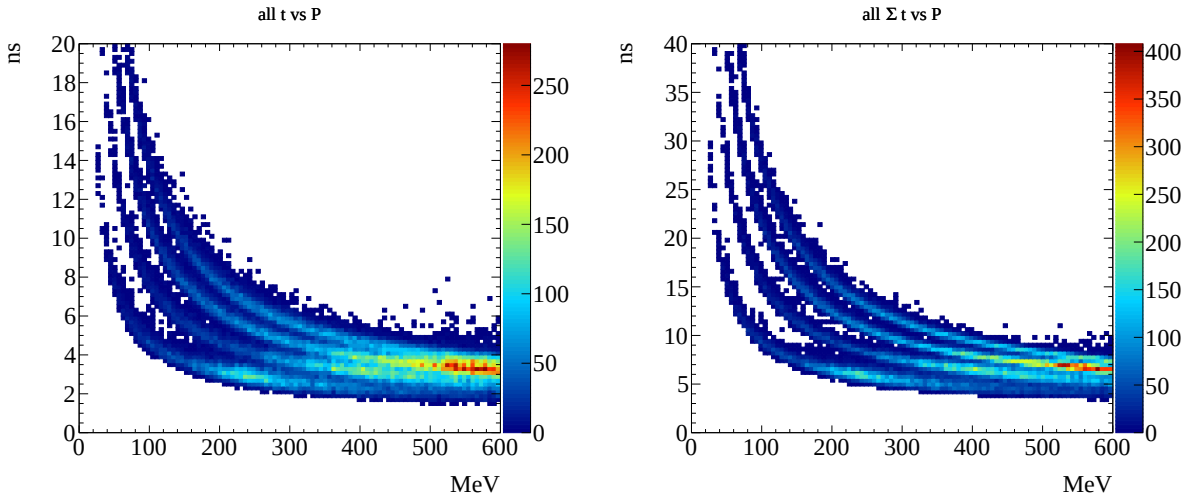

Figure 2.8: Simulated TOF for the various recoil particles vs Momentum. The TOF from just a single readout is shown on the left and the sum of the dual ended readout is shown on the right.

The front-end electrons for the SiPMs will include preamplifiers and ASICs[4] which provide both TDC and ADC readouts. The PETIROC-2A[29] ASIC provides excellent time resolution (18 ps on trigger output with 4 photoelectrons detected) and a maximum readout rate at about 40k events/s. Higher readout rates can be handled by using external digitizers by using the analog mode of operation and increase this rate by an order of magnitude. The ASIC also has the advantage of being able to tune the individual over-bias voltages with an 8-bit DAC.

The expected radiation damage to the SiPMs and scintillator material is found to be minimal over the length of the proposed experiment. We used the CLAS12 forward tagger hodoscope technical design report [28] as a very conservative baseline for this comparison. We arrived at an estimated dose of 1 krad after about 4.5 months of running. The damage to the scintillator at 100 times these radiation levels would not be problematic, even for the longest lengths of scintillator used [30]. Accumulated dose on the SiPMs leads to an increased dark current. Similarly than for scintillators, we do not expect it to be significant over the length of the experiment. The interested reader is referred to the work on SiPMs for the Hall-D detectors [31, 32]. A front-end electronics prototype will be tested for radiation hardness but we expect any damage to negligible [33].

2.3.3 Target Cell

The design of the proposed ALERT target will be very similar to the eg6 target shown in Figure 2.9. The target parameters are shown in Table 2.3 with the parameters of other existing and PAC approved targets. Note that, the proposed target has an increased radius of 6 mm compared to all the others which have 3 mm radius. This increase compared to the previous CLAS targets has been made in order to compensate for the expected increase of beam size at 11 GeV. The BONuS12 target is still presently proposed to be 3 mm in radius, if such a target is operated successfully in JLab, we will definitely consider using a smaller radius as well, but we prefer to propose here a safer option that we know will work fine.

2.4 Simulation of ALERT and reconstruction

The general detection and reconstruction scheme for ALERT is as follows. We fit the track with the drift chamber and scintillator position information to obtain the momentum over the charge. Next, using the scintillator time-of-flight, the particles are separated and identified by their mass-to-charge ratio, therefore leaving a degeneracy for the deuteron and

[4] ASIC: application-specific integrated circuit.

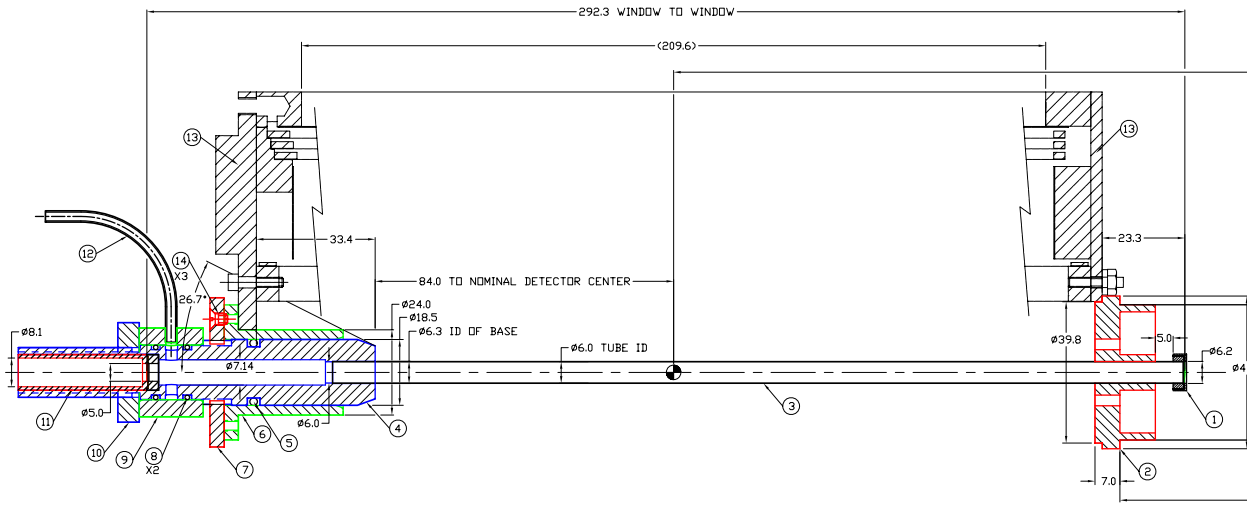

Figure 2.9: The eg6 target design drawing.

Table 2.3: Comparison of various straw targets used at JLab.The "JLab test targets" correspond to recent tests performed in JLab for the BONuS12 target, they have been tested for pressure but have never been tested with beam.

Experiment	**Length**	**Kapton wall thickness**	**Pressure**
CLAS target (eg6)	30 cm	27 µm	6.0 atm
BONuS12 (E12-06-113) target	42 cm	30 µm	7.5 atm
JLab test target 1	42 cm	30 µm	3.0 atm
JLab test target 2	42 cm	50 µm	4.5 atm
JLab test target 3	42 cm	60 µm	6.0 atm
ALERT proposed target	35 cm	25 µm	3.0 atm

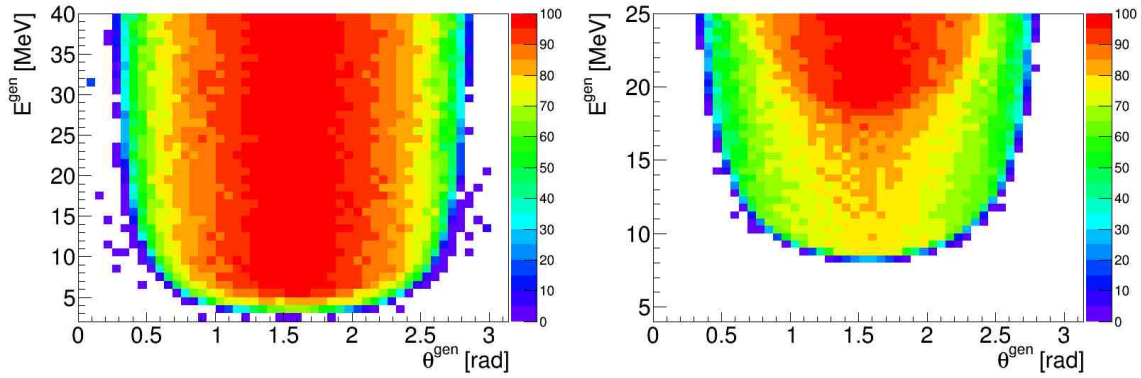

Figure 2.10: Simulated recoil detector acceptance percentage, for protons (left) and ^{4}He (right), when requiring energy deposition in the scintillators arrays.

α particles. The degeneracy between deuteron and α particles can be resolved in a few ways. The first and most simple way is to observe that an α will almost never make it to the second layer of scintillators and therefore the absence (presence) of a signal would indicate the particle is an α (deuteron). Furthermore, as will be discussed below, the measured dE/dx will differ for ^{4}He and ^{2}H, therefore, taking into account energy loss in track fitting alone can provide separation. Additionally taking further advantage of the measured total energy deposited in the scintillators can help separate the αs and deuterons.

2.4.1 Simulation of ALERT

The simulation of the recoil detector has been implemented with the full geometry and material specifications in GEANT4. It includes a 5 Tesla homogeneous solenoid field and the entire detector filled with materials as described in the previous section. In this study all recoil species are generated with the same distributions: flat in momentum from threshold up to 40 MeV ($\sim$ 250 MeV/c) for protons and about 25 MeV for other particles; isotropic angular coverage; flat distribution in z-vertex; and a radial vertex coordinate smeared around the beam line center by a Gaussian distribution of sigma equal to the expected beam radius (0.2 mm). For reconstruction, we require that the particle reaches the scintillator and obtain the acceptance averaged over the z-vertex position shown in Figure 2.10.

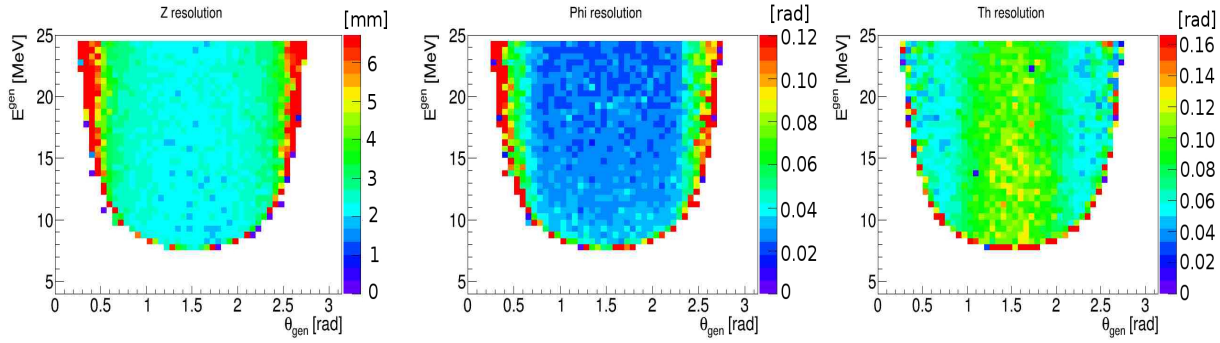

Figure 2.11: Resolutions for simulated ^{4}He: z-vertex resolution in mm (left), azimuthal (center) and polar (right) angle resolutions in radians for the lowest energy regime when the recoil track reaches the scintillator.

2.4.2 Track Fitting

The tracks are obtained using a helix fitter giving the coordinates of the vertex and the momentum of the particle. The energy deposited in the scintillators could also be used to help determine the kinetic energy of the nucleus, but is not implemented in the studies we performed here. The tracking capabilities of the recoil detector are investigated assuming a spatial resolutions of 200 µm for the drift chamber. The wires are strung in the z-direction with a stereo angle of 10°. The resulting difference between generated and reconstructed variables from simulation is shown in Figure 2.11 for ^{4}He particles. The momentum resolution for both protons and ^{4}He is presented in Figure 2.12.

2.4.3 Particle identification in ALERT

The particle identification scheme is investigated using the GEANT4 simulation as well. The scintillators have been designed to ensure a 150 ps time resolution. To determine the dE/dx resolution, measurements will be necessary for the scintillators and for the drift chamber as this depends on the detector layout, gas mixture, electronics, voltages... Nevertheless, from [34], one can assume that with 8 hits in the drift chamber and the measurements in the scintillators, the energy resolution should be at least 10%. Under these conditions, a clean separation of three of the five nuclei is shown in Figure 2.13 solely based on the time of flight measured by the scintillator compared to the reconstructed momentum from the drift chamber. We then separate ^{2}H and α using dE/dx in the drift chamber and in the scintillators.

To quantify the separation power of our device, we simulated an equal quantity of each

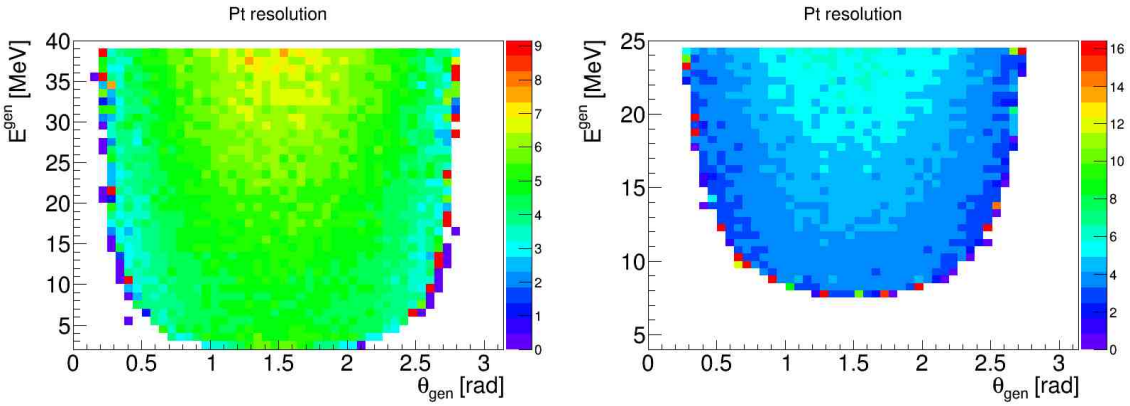

Figure 2.12: Simulated momentum resolutions (in %) as a function of energy and polar angle for protons (left) and ^{4}He (right) integrated over all z, when the recoil track reaches the scintillators array.

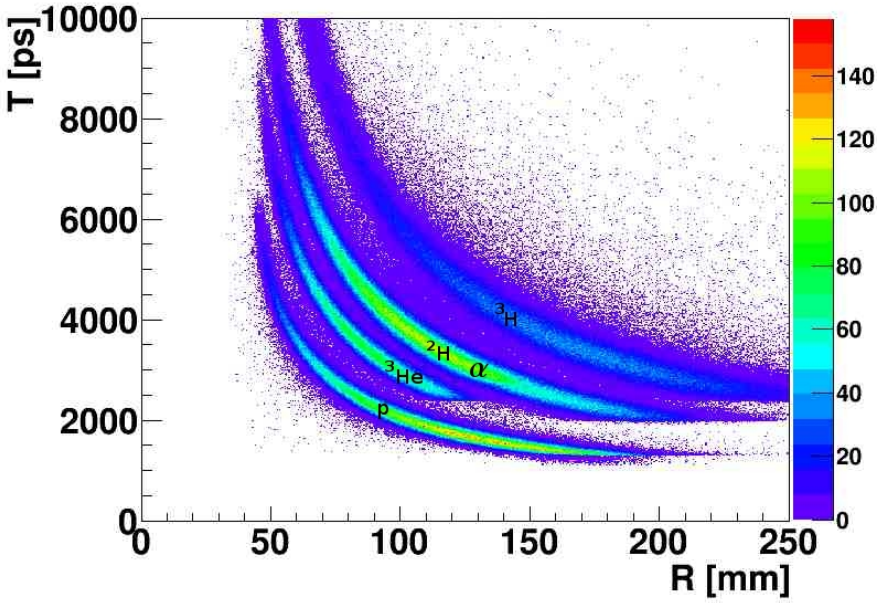

Figure 2.13: Simulated time of flight at the scintillator versus the reconstructed radius in the drift chamber. The bottom band corresponds to the proton, next band is the ^{3}He nuclei, ^{2}H and α are overlapping in the third band, the uppermost band is ^{3}H. ^{2}H and α are separated using dE/dx.

species. We obtained a particle identification efficiency of 99% for protons, 95% for ^{3}He and 98% for ^{3}H and around 90% for ^{2}H and α with equally excellent rejection factors. It is important to note that for this analysis, only the energy deposited in the scintillators was used, not the energy deposited in the drift chamber nor the path length in the scintillators, thus these numbers are very likely to be improved when using the full information[5]. This analysis indicates that the proposed reconstruction and particle identification schemes for this design are quite promising. Studies, using both simulation software and prototyping, are ongoing to determine the optimal detector parameters to minimize the detection threshold while maximizing particle identification efficiency. The resolutions presented above have been implemented in a fast Monte-Carlo used to evaluate their impact on our measurements.

2.5 Drift chamber prototype

Since the design of the drift chamber presents several challenges in term of mechanical assembly, we decided to start prototyping early. The goal is to find a design that will be easy to install and to maintain if need be, while keeping the amount of material at a minimum. This section presents the work done in Orsay to address the main questions concerning the mechanics that needed to be answered:

- How to build a stereo drift chamber with a 2 mm gap between wires?
- Can we have frames that can be quickly changed in case of a broken wire?
- How to minimize the forward structure to reduce the multiple scattering, while keeping it rigid enough to support the tension due to the wires?

For the first question, small plastic structures realized with a 3D printer were tested and wires welded on it, as shown in Figure 2.14. This demonstrated our ability to weld wires with a 2 mm gap on a curved structure.

To limit issues related to broken wires, we opted for a modular detector made of identical sectors. Each sector covers 20° of the azimuthal angle (Figure 2.15) and can be rotated around the beam axis to be separated from the other sectors. This rotation is possible due to the absence of one sector, leaving a 20° dead angle. Then, if a wire breaks, its sector can be removed independently and replaced by a spare. Plastic and metallic prototype sectors were made with 3D printers to test the assembling procedure and we have started the construction

[5]The uncertainty remains important about the resolutions that will be achieved for these extra information. So we deemed more reasonable to ignore them for now.

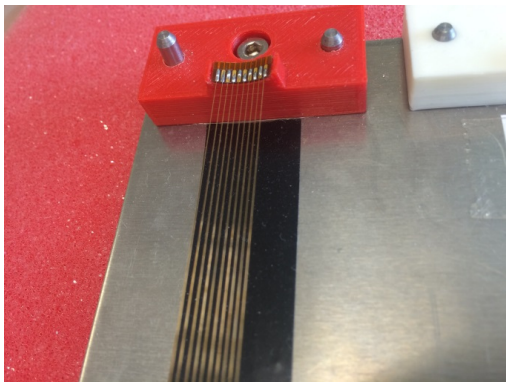

Figure 2.14: Welded wires on a curved structure with a 2 mm gap between each wire.

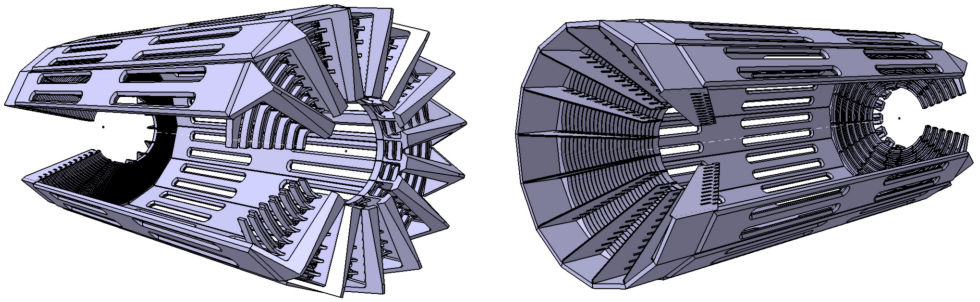

Figure 2.15: Upstream (left) and downstream (right) ends of the prototype detector in computer assisted design (CAD) with all the sectors included.

of a full size prototype of one sector. The shape of each sector is constrained by the position of the wires. It has a triangular shape on one side and due to the stereo angle, the other side looks like a pine tree with branches alternatively going left and right from a central trunk (Figure 2.16).

Finally, the material used to build the structure will be studied in details with future prototypes. Nevertheless, most recent plans are to use high rigidity plastic in the forward region and metal for the backward structure (as in Figure 2.17). The prototypes are not only designed to check the mechanical requirements summarized above but also to verify the different cell configurations, and to test the DREAM electronics (time resolution, active range, noise).

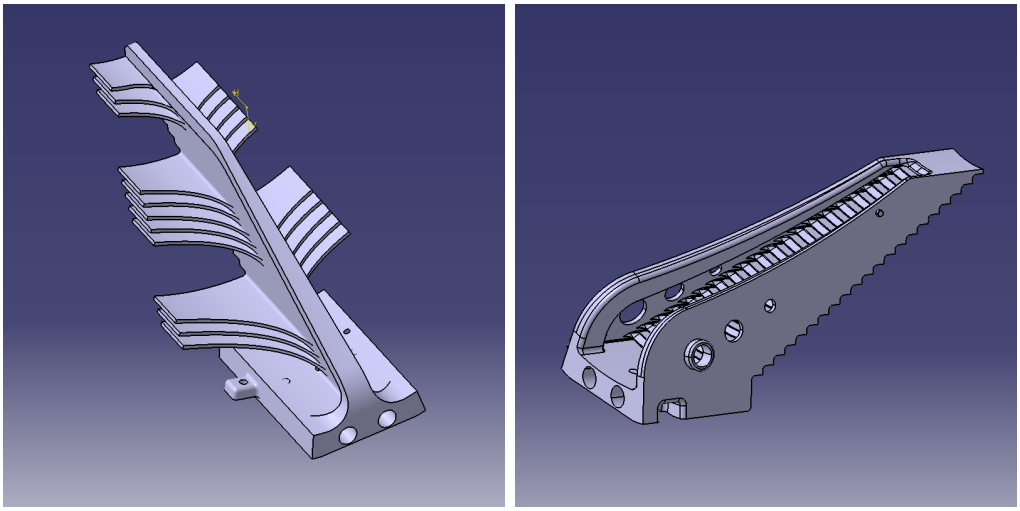

Figure 2.16: Close up on the CAD of the upstream piece (left) and downstream piece(right) of the drift chamber. Note that the design of the pieces has been optimized in comparison of what is shown in Figure 2.15.

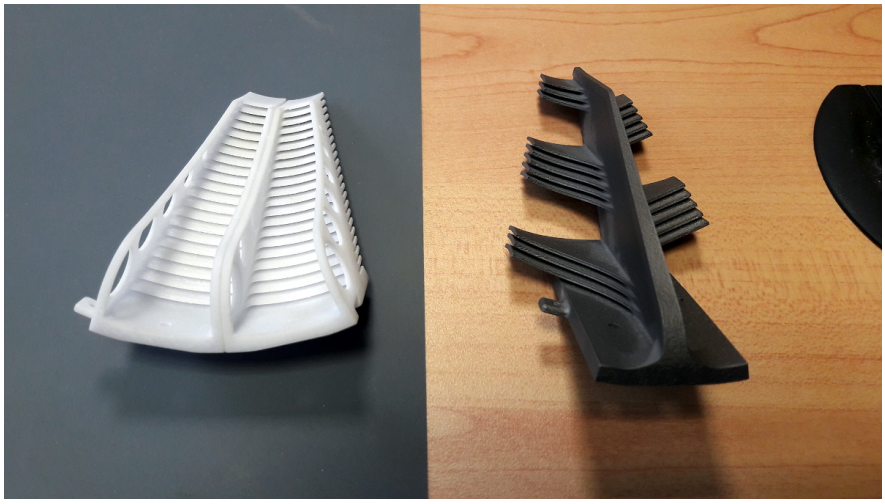

Figure 2.17: Prototypes for the mechanical parts of the drift chamber made out of plastic for the forward part and titanium for the backward.

2.6 Technical contributions from the research groups

The effort to design, build and integrate the ALERT detector is led by four research groups, Argonne National Lab (ANL), Institut de Physique Nucléaire d'Orsay (IPNO), Jefferson Lab and Temple University (TU).

Jefferson Lab is the host institution. ANL, IPNO and TU have all contributed technically to CLAS12. ANL was involved in the construction of the high-threshold Cherenkov counters (HTCC) for CLAS12. ANL has a memorandum of understanding (MOU) with JLab on taking responsibility for the HTCC light collection system including testing the photomultipliers and the magnetic shielding. For the RICH detector for CLAS12, ANL developed full GEANT-4 simulations in addition to the tracking software. ANL also developed the mechanical design of the detector support elements and entrance and exit windows in addition to the front-end electronics cooling system. IPNO took full responsibility for the design and construction of CLAS12 neutron detector (CND). The CND was successfully delivered to Jefferson Lab. TU played an important role in the refurbishment of the low threshold Cherenkov counters (LTCC), which was completed recently. All 216 photomultipliers have been coated with wavelength shifting material (p-Terphenyl) at Temple University, which resulted in a significant increase in the number of photoelectrons response.

The three institutions have already shown strong technical commitment to JLab 12 GeV upgrade, with a focus on CLAS12 and this proposal is a continuation of this commitment.

2.6.1 Argonne National Laboratory and Temple University

The ANL medium energy group is responsible for the ALERT scintillator system, including scintillation material, light collection device and electronics. First results of simulations have led to the design proposed here. This work will continue to integrate the scintillator system with the wire chamber. ANL will collaborate closely with Temple University to test the light detection system. Both institutions will be responsible to assemble and test the detector.

Argonne will provide the electronics and technical support required to integrate the scintillator detector system into the CLAS12 DAQ. The effort will minimize the effort required on the part of the Hall B staff.

2.6.2 Institut de Physique Nucléaire d'Orsay

The Institut de Physique Nucléaire d'Orsay is responsible for the wire chamber and the mechanical structure of the detector design and construction. As shown in the proposal, this work has already started, a first prototype is being built to test different cell forms, wire material, wire thickness, pressure, etc. This experience will lead to a complete design of the ALERT detector integrating the scintillator built at ANL, the gas distribution system and the electronic connections.

In partnership with *CEA Saclay*, IPN Orsay will also test the use of the DREAM front-end chip for the wire chamber. Preliminary tests were successful and will continue. The integration of the chip with CLAS12 is expected to be done by the *CEA Saclay*, since they use the same chip to readout the CLAS12 MVT. Adaptations to the DAQ necessary when the MVT will be replaced by ALERT will be performed by the staff of IPN Orsay.

2.6.3 Jefferson Laboratory

We expect Jefferson Lab to help with the configuration of the beam line. This will include the following items.

Beam Dump Upgrade The maximum beam current will be around 1000 nA for the production runs at 10^{35} $cm^{-2}s^{-1}$, which is not common for Hall-B. To run above 500 nA the "beam blocker" will need to be upgraded to handle higher power. The beam blocker attenuates the beam seen by the Faraday cup. This blocker is constructed of copper and is water cooled. Hall B staff have indicated that this is a rather straightforward engineering task and has no significant associated costs [35].

Straw Target We also expect JLab to design and build the target for the experiment as it will be a very similar target as the ones build for CLAS BONuS and eg6 runs. See section 2.3.3 for more details.

Mechanical Integration We also expect Jefferson Laboratory to provide assistance in the detector installation in the Hall. This will include providing designers at ANL and IPNO with the technical drawings required to integrate ALERT with CLAS12. We will also need some coordination between designers to validate the mechanical integration.

CLAS12 DAQ Integration We also will need assistance in connecting the electronics of ALERT to the CLAS12 data acquisition and trigger systems. This will also include help integrating the slow controls into the EPICs system.

Summary and Answers to PAC44

Answers to PAC44 issues

Issues:

The Drift Chamber/scintillator technology needs to be demonstrated. We observe that a strong program of prototype studies is already underway.

Answer: We feel the technology has no major unknowns, wire chambers and scintillators have been used for decades as detectors of low energy nuclei and their properties have been well established. We present in the proposal a conceptual design demonstrating the feasibility of the detector, it is common practice to work on the optimization of a certain number of parameters after the proposal is approved. In particular, because it is easier to fund and man a project that has an approved status than a future proposal. Nevertheless, we remain open to discuss the topic in more depth if the committee has any concerns.

The TAC report voiced concerns about the length of the straw cell target and the substantial effort needed to integrate the DAQ for this detector into the CLAS12 DAQ.

Answer: The TAC and PAC44 raised concerns about the target cell. We have added extra discussion in section 2.3.3, which includes a table of existing or planned targets that are similar to the one we proposed. In summary, our proposed target is twice as wide as the ones used in the 6 GeV era for the BONuS and eg6 run and should therefore cause no issues. Note that the experiment 12-06-113 (BONuS12) is approved with a longer and thinner target. Their design will be reviewed by JLab for their experiment readiness review (ERR) before the PAC45 meeting. The result of this review should settle the question, but in any case, we propose a safer solution based on the successful experiments of the 6 GeV era.

The TAC and PAC44 raised issues regarding integration of ALERT into the CLAS12 DAQ. First, they raised a concern that the resources necessary for this integration are not

clearly identified. We have added text in section 2.6.3 outlining the resources provided by each group and the technical support they are expected to provide. Secondly, they mentioned a concern about the "substantial effort needed to integrate the DAQ for this detector into the CLAS12 DAQ". We want to emphasize that the read-out systems for ALERT are already being used in the CLAS12 DAQ to readout Micromegas detectors. Therefore, we will use and build on the experience gained from these systems.

The proposal does not clearly identify the resources (beyond generic JLAB/CLAS12 effort) necessary for DAQ integration which may be a substantial project.

Answer: As mentioned above, we do not feel this contribution is major, nevertheless we made this part clearer in the proposal.

During review the collaboration discovered an error in converting the luminosity to beam current. This resulted in a revision that will either require doubling the current or the target density. The beam current change would require changes to the Hall B beam dump, while raising the target density could impact the physics reach of the experiment by raising the minimum momentum threshold.

Answer: During the PAC44 proposal submission process the wrong beam current was requested. It was a factor of 2 too low. This increased beam current brought into contention the issue of possible Hall B beam current limits. We chose to use the higher beam current in this new version. Based on discussions with the Hall-B and accelerator staff, the only necessary upgrade necessary to run at 1 µA is with the Hall-B beam blocker.

The precise interplay between final state interactions (FSI) and the tails of the initial state momentum distribution in DVCS on 4He was a topic of some debate. The collaboration makes an argument that the excellent acceptance of the apparatus allows novel constraints that allow selection of kinematic ranges where FSI is suppressed. While the originally suggested method to unambiguously identify areas of FSI was revised during the review, the committee remains unconvinced that the new kinematic selections suggested do not also cut into interesting regimes for the initial state kinematics. The committee believes that this is model dependent and would like to see more quantitative arguments than were provided in this version of the proposal.

Answer: We acknowledge there was an overstatement of the possibilities of the Tagged-DVCS proposal on this topic, this has been corrected. We now show a reduction, in opposition to the complete suppression previously claimed, in events that differ from the PWIA result. This finding is based on a simulation using a simple model of FSIs together with a Monte-Carlo event generator.

Summary:

The committee was generally enthusiastic about the diverse science program presented in this proposal; in particular the tagged EMC studies and the unique study of coherent GPD's on the 4He nucleus. However, the substantial modifications made in the proposal during review indicate that it could be substantially improved on a reasonably short time scale. We would welcome a new proposal that addresses the issues identified by the committee and by the collaboration.

Answer: We hope that the new proposals will answer all the questions raised by the PAC44 and will make the physics case even more compelling.

We also note that there are multiple experiments, proposed and approved, to study the EMC effect, including several with novel methods of studying the recoil system. We appreciate the comparisons of recoil technologies in this proposal and would welcome a broader physics discussion of how the proposed measurements contribute to a lab-wide strategy for exploring the EMC effect.

Answer: While no strategy document has been drafted after them, we want to point out to the PAC that the community of physicist interested by the partonic structure of nuclei meets regularly, with often a large focus on what can be done at JLab (see workshops at Trento[6], Miami[7], MIT[8], and Orsay[9] for example). Nonetheless, we added in the tagged EMC proposal summary an extension about the 12 GeV approved experiments related to the EMC effect. This short annex will hopefully clarify the context and the uniqueness of the present experiments.

Summary and Beam Time Request

In summary, there is a broad experimental program to be carried out using the CLAS12 and ALERT detectors. This fourth proposal only gives a flavor of the many possibilities. The ALERT collaboration has every intention of mining the data that will be collected during the ALERT run and advance our understanding of nuclear QCD. This proposal focuses on exclusive π^0 production off ^{4}He, coherent exclusive DVCS off deuteron and DVCS in three-body break up reactions. These topics are closely connected to the ones proposed in the three proposals which compose the ALERT run group. There is no additional beam time request and these three measurements are perfectly compatible with the running conditions of the ALERT run group.

[6]New Directions in Nuclear Deep Inelastic Scattering http://www.ectstar.eu/node/1221

[7]Next generation nuclear physics with JLab12 and EIC https://www.jlab.org/indico/event/121/

[8]Quantitative challenges in EMC and SRC Research and Data-Mining http://web.mit.edu/schmidta/www/src_workshop/

[9]Partons and Nuclei https://indico.in2p3.fr/event/14438/

Appendix A

Twist-3 electroproduction cross-section off a spinless target

The differential cross section for real photon electroproduction of a longitudinally-polarized electron beam on a spin-zero target can be expressed as [36]:

$$\frac{d^5\sigma_\lambda}{dx_A dQ^2 dt d\phi_e d\phi} = \frac{\alpha^3}{16\pi^2}\frac{x_A\, y^2}{Q^4\sqrt{1+\varepsilon^2}}\frac{|\mathcal{T}_{BH}|^2 + |\mathcal{T}^\lambda_{DVCS}|^2 + \mathcal{I}^\lambda_{BH*DVCS}}{e^6} \tag{A.1}$$

where $y = \frac{p\cdot q}{p\cdot k}$, $\varepsilon = \frac{2x_A M_A}{Q}$ and $x_A = \frac{Q^2}{2p\cdot q}$. The different amplitudes can be written as:

$$|\mathcal{T}_{BH}|^2 = \frac{e^6(1+\varepsilon^2)^{-2}}{x_A^2 y^2 t \mathcal{P}_1(\phi)\mathcal{P}_2(\phi)}\sum_{n=0}^{2} c_n^{BH}\cos(n\phi) \tag{A.2}$$

$$|\mathcal{T}_{DVCS}|^2 = \frac{e^6}{y^2 Q^2}\sum_{n=0}^{2}\left(c_n^{DVCS}\cos(n\phi) + \lambda s_n^{DVCS}\sin(n\phi)\right) \tag{A.3}$$

$$\mathcal{I}_{BH*DVCS} = \frac{\pm e^6}{x_A y^3 t\, \mathcal{P}_1(\phi)\mathcal{P}_2(\phi)}\sum_{n=0}^{3}\left(c_n^I\cos(n\phi) + \lambda s_n^I\sin(n\phi)\right) \tag{A.4}$$

The beam-spin asymmetry (A_{LU}) with the two opposite helicities of a longitudinally-polarized electron beam (L) on a spin-zero target (U) can be written as:

$$A_{LU} = \frac{D_1 \sum_{n=1}^{2} s_n^{DVCS} \sin(n\phi) + D_2 \sum_{n=1}^{3} s_n^{I} \sin(n\phi)}{\sum_{n=0}^{n=2} c_n^{BH} \cos(n\phi) + D_1 \sum_{n=0}^{n=2} c_n^{DVCS} \cos(n\phi) + D_2 \sum_{n=0}^{n=3} c_n^{I} \cos(n\phi)} \tag{A.5}$$

with the kinematical variables $D_1 = \frac{x_A^2 t (1+\varepsilon^2)^2}{Q^2} P_1(\phi) P_2(\phi)$ and $D_2 = \frac{x_A (1+\varepsilon^2)^2}{y}$.

At twist-3, the $|\mathcal{T}_{DVCS}|^2$ writes as a function of the following Fourier coefficients

$$c_0^{\rm DVCS} = 2\frac{2-2y+y^2+\frac{\varepsilon^2}{2}y^2}{1+\varepsilon^2}\mathcal{C}^{\rm DVCS}(\mathcal{H},\mathcal{H}^*;\mathcal{H}_T,\mathcal{H}_T^*) + \frac{16K^2\mathcal{H}_{\rm eff}\mathcal{H}_{\rm eff}^*}{(2-x_B)^2(1+\varepsilon^2)}\,, \tag{A.6}$$

$$\left\{ \begin{matrix} c_1^{\rm DVCS} \\ s_1^{\rm DVCS} \end{matrix} \right\} = \frac{8K}{(2-x_B)(1+\varepsilon^2)} \left\{ \begin{matrix} (2-y)\,\Re{\rm e} \\ -\lambda y\sqrt{1+\varepsilon^2}\,\Im{\rm m} \end{matrix} \right\} \mathcal{C}^{\rm DVCS}\left(\mathcal{H}^{\rm eff};\mathcal{H}^*;\mathcal{H}_T^*\right)\,, \tag{A.7}$$

$$c_2^{\rm DVCS} = \frac{16\mathcal{Q}^2K^2}{M^2(2-x_B)^2(1+\varepsilon^2)}\Re{\rm e}\,\mathcal{C}_T^{\rm DVCS}\left(\mathcal{H},\mathcal{H}_T^*\right)\,. \tag{A.8}$$

where the bilinear CFFs and the effective twist-three CFF $\mathcal{H}_3^{\rm eff}$ read:

$$\begin{aligned} \mathcal{C}^{\rm DVCS}\left(\mathcal{H},\mathcal{H}^*,\mathcal{H}_T,\mathcal{H}_T^*\right) &= \mathcal{H}\mathcal{H}^* + \frac{\widetilde{K}^4}{(2-x_B)^4}\mathcal{H}_T\mathcal{H}_T^*\,, \\ \mathcal{C}^{\rm DVCS}\left(\mathcal{H}_{\rm eff};\mathcal{H}^*;\mathcal{H}_T^*\right) &= \mathcal{H}_{\rm eff}\left(\mathcal{H}^* + \frac{2\widetilde{K}^2}{M^2(2-x_B)^2}\mathcal{H}_T^*\right) \\ \mathcal{C}_T^{\rm DVCS}\left(\mathcal{H},\mathcal{H}_T^*\right) &= \mathcal{H}\mathcal{H}_T^*\,. \end{aligned} \tag{A.9}$$

$$\mathcal{H}^{\rm eff} \equiv -2\xi\left(\frac{1}{1+\xi}\mathcal{H} + \mathcal{H}_+^3 - \mathcal{H}_-^3\right)\,, \tag{A.10}$$

with the CFFs $\mathcal{H}_\pm^3$ related to functions $H_\pm^3$ given by a convolution of the twist-two GPD H and the so-called Wandzura-Wilczek kernel provided one neglects dynamical quark-gluon-quark correlation functions.

The interference amplitude coefficients are written as:

$$c_n^{\mathcal{I}} = C_{++}(n)\,\Re\mathrm{e}\,\mathcal{C}^{\mathcal{I}}\left(\mathcal{H}\right) + \frac{\sqrt{2}}{2-x_B}\,\frac{\widetilde{K}}{Q}\,C_{0+}(n)\,\Re\mathrm{e}\,\mathcal{C}^{\mathcal{I}}\left(\mathcal{H}_3^{\mathrm{eff}}\right) + \frac{2}{(2-x_B)^2}\,\frac{\widetilde{K}^2}{M^2}\,C_{-+}(n)\,\Re\mathrm{e}\,\mathcal{C}^{\mathcal{I}}\left(\mathcal{H}_T\right)\,, \tag{A.11}$$

$$s_n^{\mathcal{I}} = S_{++}(n)\,\Im\mathrm{m}\,\mathcal{C}^{\mathcal{I}}\left(\mathcal{H}\right) + \frac{\sqrt{2}}{2-x_B}\,\frac{\widetilde{K}}{Q}\,S_{0+}(n)\,\Im\mathrm{m}\,\mathcal{C}^{\mathcal{I}}\left(\mathcal{H}_3^{\mathrm{eff}}\right) + \frac{2}{(2-x_B)^2}\,\frac{\widetilde{K}^2}{M^2}\,S_{-+}(n)\,\Im\mathrm{m}\,\mathcal{C}^{\mathcal{I}}\left(\mathcal{H}_T\right)\,, \tag{A.12}$$

with the CFF components

$$\mathcal{C}^{\mathcal{I}}(\mathcal{H}) = F\mathcal{H}\,, \qquad \mathcal{C}_T^{\mathcal{I}} = F\mathcal{H}_T\,. \tag{A.13}$$

The individual Fourier harmonics are detailed in the following sections.

The explicit expressions for the Fourier coefficients entering the leptonic part of the interference

term are presented herein. For the transverse-transverse harmonics we have

$$
\begin{aligned}
C_{++}(n=0) &= -\frac{4(2-y)\left(1+\sqrt{1+\varepsilon^2}\right)}{(1+\varepsilon^2)^2}\left\{\frac{\widetilde{K}^2}{Q^2}\frac{(2-y)^2}{\sqrt{1+\varepsilon^2}}\right. \\
&\left. + \frac{t}{Q^2}\left(1-y-\frac{\varepsilon^2}{4}y^2\right)(2-x_B)\left(1+\frac{2x_B\left(2-x_B+\frac{\sqrt{1+\varepsilon^2}-1}{2}+\frac{\varepsilon^2}{2x_B}\right)\frac{t}{Q^2}+\varepsilon^2}{(2-x_B)(1+\sqrt{1+\varepsilon^2})}\right)\right\}, \\
C_{++}(n=1) &= \frac{-16K\left(1-y-\frac{\varepsilon^2}{4}y^2\right)}{(1+\varepsilon^2)^{5/2}}\left\{\left(1+(1-x_B)\frac{\sqrt{\varepsilon^2+1}-1}{2x_B}+\frac{\varepsilon^2}{4x_B}\right)\frac{x_Bt}{Q^2}-\frac{3\varepsilon^2}{4}\right\} \\
&\quad -4K\left(2-2y+y^2+\frac{\varepsilon^2}{2}y^2\right)\frac{1+\sqrt{1+\varepsilon^2}-\varepsilon^2}{(1+\varepsilon^2)^{5/2}}\left\{1-(1-3x_B)\frac{t}{Q^2}\right. \\
&\qquad \left. +\frac{1-\sqrt{1+\varepsilon^2}+3\varepsilon^2}{1+\sqrt{1+\varepsilon^2}-\varepsilon^2}\frac{x_Bt}{Q^2}\right\}, \\
C_{++}(n=2) &= \frac{8(2-y)\left(1-y-\frac{\varepsilon^2}{4}y^2\right)}{(1+\varepsilon^2)^2}\left\{\frac{2\varepsilon^2}{1+\varepsilon^2+\sqrt{1+\varepsilon^2}}\frac{\widetilde{K}^2}{Q^2}\right. \\
&\qquad \left. +\frac{x_Bt\,t'}{Q^4}\left(1-x_B-\frac{\sqrt{1+\varepsilon^2}-1}{2}+\frac{\varepsilon^2}{2x_B}\right)\right\}, \\
C_{++}(n=3) &= -8K\left(1-y-\frac{\varepsilon^2}{4}y^2\right)\frac{\sqrt{1+\varepsilon^2}-1}{(1+\varepsilon^2)^{5/2}}\left\{(1-x_B)\frac{t}{Q^2}+\frac{\sqrt{1+\varepsilon^2}-1}{2}\left(1+\frac{t}{Q^2}\right)\right\}, \\
S_{++}(n=1) &= -\frac{8K(2-y)y}{1+\varepsilon^2}\left\{1+\frac{1-x_B+\frac{\sqrt{1+\varepsilon^2}-1}{2}}{1+\varepsilon^2}\frac{t'}{Q^2}\right\}, \\
S_{++}(n=2) & \\
&= \frac{4\left(1-y-\frac{\varepsilon^2}{4}y^2\right)y}{(1+\varepsilon^2)^{3/2}}\left(1+\sqrt{1+\varepsilon^2}-2x_B\right)\frac{t'}{Q^2}\left\{\frac{\varepsilon^2-x_B(\sqrt{1+\varepsilon^2}-1)}{1+\sqrt{\varepsilon^2+1}-2x_B}-\frac{2x_B+\varepsilon^2}{2\sqrt{1+\varepsilon^2}}\frac{t'}{Q^2}\right\},
\end{aligned}
\tag{A.14}
$$

while the longitudinal-transverse ones,

$$C_{0+}(n=0) = \frac{12\sqrt{2}K(2-y)\sqrt{1-y-\frac{\varepsilon^2}{4}y^2}}{(1+\varepsilon^2)^{5/2}}\left\{\varepsilon^2+\frac{2-6x_B-\varepsilon^2}{3}\frac{t}{Q^2}\right\}, \tag{A.15}$$

$$C_{0+}(n=1) = \frac{8\sqrt{2}\sqrt{1-y-\frac{\varepsilon^2}{4}y^2}}{(1+\varepsilon^2)^2}\left\{(2-y)^2\frac{t'}{Q^2}\left(1-x_B+\frac{(1-x_B)x_B+\frac{\varepsilon^2}{4}}{\sqrt{1+\varepsilon^2}}\frac{t'}{Q^2}\right)\right.$$
$$\left.+\frac{1-y-\frac{\varepsilon^2}{4}y^2}{\sqrt{1+\varepsilon^2}}\left(1-(1-2x_B)\frac{t}{Q^2}\right)\left(\varepsilon^2-2\left(1+\frac{\varepsilon^2}{2x_B}\right)\frac{x_Bt}{Q^2}\right)\right\},$$

$$C_{0+}(n=2) = -\frac{8\sqrt{2}K(2-y)\sqrt{1-y-\frac{\varepsilon^2}{4}y^2}}{(1+\varepsilon^2)^{5/2}}\left(1+\frac{\varepsilon^2}{2}\right)\left\{1+\frac{1+\frac{\varepsilon^2}{2x_B}}{1+\frac{\varepsilon^2}{2}}\frac{x_Bt}{Q^2}\right\},$$

$$S_{0+}(n=1) = -\frac{8\sqrt{2}(2-y)y\sqrt{1-y-\frac{\varepsilon^2}{4}y^2}}{(1+\varepsilon^2)^2}\frac{\widetilde{K}^2}{Q^2},$$

$$S_{0+}(n=2) = -\frac{8\sqrt{2}Ky\sqrt{1-y-\frac{\varepsilon^2}{4}y^2}}{(1+\varepsilon^2)^2}\left(1+\frac{\varepsilon^2}{2}\right)\left\{1+\frac{1+\frac{\varepsilon^2}{2x_B}}{1+\frac{\varepsilon^2}{2}}\frac{x_Bt}{Q^2}\right\}.$$

Finally, the helicity-flip transverse-transverse coefficients are

$$
\begin{aligned}
C_{-+}(n=0) &= \frac{8(2-y)}{(1+\varepsilon^2)^{3/2}}\Bigg\{(2-y)^2\frac{\sqrt{1+\varepsilon^2}-1}{2(1+\varepsilon^2)}\frac{\widetilde{K}^2}{Q^2} \\
&\quad + \frac{1-y-\frac{\varepsilon^2}{4}y^2}{\sqrt{1+\varepsilon^2}}\left(1-x_B-\frac{\sqrt{1+\varepsilon^2}-1}{2}+\frac{\varepsilon^2}{2x_B}\right)\frac{x_B t\, t'}{Q^4}\Bigg\}, \\
C_{-+}(n=1) &= \frac{8K}{(1+\varepsilon^2)^{3/2}}\Bigg\{(2-y)^2\frac{2-\sqrt{1+\varepsilon^2}}{1+\varepsilon^2}\left(\frac{\sqrt{1+\varepsilon^2}-1+\varepsilon^2}{2\left(2-\sqrt{1+\varepsilon^2}\right)}\left(1-\frac{t}{Q^2}\right)-\frac{x_B t}{Q^2}\right) \\
&\quad + 2\frac{1-y-\frac{\varepsilon^2}{4}y^2}{\sqrt{1+\varepsilon^2}}\left(\frac{1-\sqrt{1+\varepsilon^2}+\frac{\varepsilon^2}{2}}{2\sqrt{1+\varepsilon^2}}+\frac{t}{Q^2}\left(1-\frac{3x_B}{2}+\frac{x_B+\frac{\varepsilon^2}{2}}{2\sqrt{1+\varepsilon^2}}\right)\right)\Bigg\}, \\
C_{-+}(n=2) &= 4(2-y)\left(1-y-\frac{\varepsilon^2}{4}y^2\right)\frac{1+\sqrt{1+\varepsilon^2}}{(1+\varepsilon^2)^{5/2}}\Bigg\{(2-3x_B)\frac{t}{Q^2} \\
&\quad + \left(1-2x_B+\frac{2(1-x_B)}{1+\sqrt{1+\varepsilon^2}}\right)\frac{x_B t^2}{Q^4}+\left(1+\frac{\sqrt{1+\varepsilon^2}+x_B+(1-x_B)\frac{t}{Q^2}}{1+\sqrt{1+\varepsilon^2}}\frac{t}{Q^2}\right)\varepsilon^2\Bigg\}, \\
C_{-+}(n=3) &= -8K\left(1-y-\frac{\varepsilon^2}{4}y^2\right)\frac{1+\sqrt{1+\varepsilon^2}+\frac{\varepsilon^2}{2}}{(1+\varepsilon^2)^{5/2}}\left\{1+\frac{1+\sqrt{1+\varepsilon^2}+\frac{\varepsilon^2}{2x_B}}{1+\sqrt{1+\varepsilon^2}+\frac{\varepsilon^2}{2}}\frac{x_B t}{Q^2}\right\}, \\
S_{-+}(n=1) &= -\frac{4K(2-y)y}{(1+\varepsilon^2)^2}\left\{1-\sqrt{1+\varepsilon^2}+2\varepsilon^2-2\left(1+\frac{\sqrt{1+\varepsilon^2}-1}{2x_B}\right)\frac{x_B t}{Q^2}\right\}, \\
S_{-+}(n=2) &= -2y\left(1-y-\frac{\varepsilon^2}{4}y^2\right)\frac{1+\sqrt{1+\varepsilon^2}}{(1+\varepsilon^2)^2}\left(\varepsilon^2-2\left(1+\frac{\varepsilon^2}{2x_B}\right)\frac{x_B t}{Q^2}\right) \\
&\quad \times\left\{1+\frac{\sqrt{1+\varepsilon^2}-1+2x_B}{1+\sqrt{1+\varepsilon^2}}\frac{t}{Q^2}\right\}.
\end{aligned}
\tag{A.16}
$$

Bibliography

[1] K. Hafidi *et al.*, "Nuclear Exclusive and Semi-inclusive Physics with a New CLAS12 Low Energy Recoil Detector (LOI-10-009)," *A Letter of Intent to PAC 35*, 2010.

[2] X. Ji, X. Xiong, and F. Yuan, "Transverse Polarization of the Nucleon in Parton Picture," *Phys. Lett.*, vol. B717, pp. 214–218, 2012.

[3] M. Diehl, "Generalized parton distributions with helicity flip," *Eur. Phys. J.*, vol. C19, pp. 485–492, 2001.

[4] S. Ahmad, G. R. Goldstein, and S. Liuti, "Nucleon Tensor Charge from Exclusive pi**o Electroproduction," *Phys. Rev.*, vol. D79, p. 054014, 2009.

[5] S. V. Goloskokov and P. Kroll, "Transversity in hard exclusive electroproduction of pseudoscalar mesons," *Eur. Phys. J.*, vol. A47, p. 112, 2011.

[6] G. R. Goldstein, J. O. G. Hernandez, and S. Liuti, "Easy as π^o: On the Interpretation of Recent Electroproduction Results," *J. Phys.*, vol. G39, p. 115001, 2012.

[7] G. R. Goldstein, J. O. G. Hernandez, and S. Liuti, "Flexible Parametrization of Generalized Parton Distributions: The Chiral-Odd Sector," *Phys. Rev.*, vol. D91, no. 11, p. 114013, 2015.

[8] P. Kroll, "Hard exclusive pion leptoproduction," 2016.

[9] R. Boussarie, B. Pire, L. Szymanowski, and S. Wallon, "Revealing transversity GPDs through the photoproduction of a photon and a ρ meson," *EPJ Web Conf.*, vol. 112, p. 01006, 2016.

[10] I. Bedlinskiy *et al.*, "Exclusive π^0 electroproduction at $W > 2$ GeV with CLAS," *Phys. Rev.*, vol. C90, no. 2, p. 025205, 2014. [Addendum: Phys. Rev.C90,no.3,039901(2014)].

[11] A. Kim *et al.*, "Target and Double Spin Asymmetries of Deeply Virtual π^0 Production with a Longitudinally Polarized Proton Target and CLAS," 2015.

[12] L. Favart, M. Guidal, T. Horn, and P. Kroll, "Deeply Virtual Meson Production on the nucleon," 2015.

[13] G. R. Goldstein, J. O. G. Hernandez, and S. Liuti, "Flavor dependence of chiral odd generalized parton distributions and the tensor charge from the analysis of combined π^0 and η exclusive electroproduction data," 2014.

[14] C. Lorce and B. Pasquini, "Quark Wigner Distributions and Orbital Angular Momentum," *Phys. Rev.*, vol. D84, p. 014015, 2011.

[15] I. C. Cloet, W. Bentz, and A. W. Thomas, "EMC and polarized EMC effects in nuclei," *Phys. Lett.*, vol. B642, pp. 210–217, 2006.

[16] E. R. Berger, F. Cano, M. Diehl, and B. Pire, "Generalized parton distributions in the deuteron," *Phys. Rev. Lett.*, vol. 87, p. 142302, 2001.

[17] A. Kirchner and D. Mueller, "Deeply virtual Compton scattering off nuclei," *Eur. Phys. J.*, vol. C32, pp. 347–375, 2003.

[18] M. Amarian *et al.*, "Deeply Virtual Compton Scattering on the Deuteron with CLAS at 6 GeV (PR06-015)," *A proposal to PAC 29*, 2006.

[19] R. B. Wiringa, R. Schiavilla, S. C. Pieper, and J. Carlson, "Nucleon and nucleon-pair momentum distributions in $A \leq 12$ nuclei," *Phys. Rev.*, vol. C89, no. 2, p. 024305, 2014.

[20] "CLAS12 Technical Design Report," 2008.

[21] H. Fenker *et al.*, "BoNus: Development and use of a radial TPC using cylindrical GEMs," *Nucl. Instrum. Meth.*, vol. A592, pp. 273–286, 2008.

[22] M. Amaryan *et al.*, "The Structure of the Free Neutron at Large x-Bjorken (PR12-06-113)," *A proposal to PAC 30*, 2006.

[23] J. Peyré, B. Genolini, and J. Poutas, "A Full-Scale Prototype for the Tracking Chambers of the ALICE Muon Spectrometer," 1998.

[24] T. Abe *et al.*, "Belle II Technical Design Report," 2010.

[25] E. Etzion *et al.*, "The Certification of ATLAS Thin Gap Chambers Produced in Israel and China," 2004.

[26] S. Biagi, "Monte Carlo simulation of electron drift and diffusion in counting gases under the influence of electric and magnetic fields," *Nucl.Instrum.Meth.*, vol. A421, pp. 234–240, 1999.

[27] C. Ciofi degli Atti *et al.*, "The readout system for the clas12 micromegas vertex tracker," in *2014 19th IEEE-NPSS Real Time Conference*, pp. 1–11, May 2014.

[28] T. C. Collaboration, "Clas12 forward tagger (ft) technical design report." https://www.jlab.org/Hall-B/clas12-web/docs/ft-tdr.2.0.pdf, 2012. Online; accessed 29 January 2016.

[29] "Petiroc-2a." http://www.weeroc.com/en/products/petiroc-2. Accessed: 2017-05-15.

[30] C. Zorn, "A pedestrian's guide to radiation damage in plastic scintillators," *Nucl. Phys. Proc. Suppl.*, vol. 32, pp. 377–383, 1993.

[31] Y. Qiang, C. Zorn, F. Barbosa, and E. Smith, "Radiation Hardness Tests of SiPMs for the JLab Hall D Barrel Calorimeter," *Nucl. Instrum. Meth.*, vol. A698, pp. 234–241, 2013.

[32] Y. Qiang, C. Zorn, F. Barbosa, and E. Smith, "Neutron radiation hardness tests of SiPMs," *AIP Conf. Proc.*, vol. 1560, pp. 703–705, 2013.

[33] S. Ahmad. Private communication, May 2017. Weeroc SAS.

[34] K. Emi *et al.*, "Study of a dE/ dx measurement and the gas-gain saturation by a prototype drift chamber for the BELLE-CDC," *Nucl. Instrum. Meth.*, vol. A379, pp. 225–231, 1996.

[35] S. Stepanyan and A. P. Freyberger. Private communication, May 2017.

[36] A. V. Belitsky and D. Mueller, "Refined analysis of photon leptoproduction off spinless target," *Phys. Rev.*, vol. D79, p. 014017, 2009.